Design and Analysis of Surface-Plasmon-Resonance-Based Photonic Quasi-Crystal Fiber Biosensor for High-Refractive-Index Liquid Analytes

Suoda Chu ⓘ, K. Nakkeeran ⓘ, *Senior Member, IEEE*, Abdosllam M. Abobaker, *Member, IEEE*,
Sumeet S. Aphale ⓘ, *Senior Member, IEEE*, P. Ramesh Babu, and K. Senthilnathan ⓘ

Abstract—We propose a sixfold photonic quasi-crystal fiber with a trapezoidal analyte channel based on surface plasmon resonance for the detection of high-refractive-index (RI) liquid analytes and numerically analyze its sensing performance for different liquid analyte refractive indices and heights using the finite-element method. In contrast to the common D-shaped structure photonic crystal fiber, we design a trapezoidal analyte channel to investigate the role of the sample liquid height within the channel and discussed the feasibility of the fabrication process. We find that with various liquid analyte heights ratios of 20%, 25%, 30%, and 50% of the maximum channel height, the proposed biosensor exhibits linear sensing performance with a maximum RI sensitivity of 4400, 6100, 8000, and 17000 nm/RIU, respectively, for analytes RI range of 1.44–1.57, 1.41–1.51, 1.40–1.49, and 1.40–1.44. This sensor is suitable to detect various high RI chemicals, biochemicals, and organic chemical samples. Owing to its simple structure of the proposed biosensor with promising linear sensing performance, we envisage that this biosensor could turn out to be a versatile and competitive instrument for the detection of high-RI liquid analytes.

Index Terms—Biosensor, photonic quasi-crystal fiber, refractive index sensor, sensitivity, surface plasmon resonance.

I. INTRODUCTION

IT IS well established that the surface plasmon resonance (SPR) based optical fiber biosensors are simple and compact probe designed for high sensitivity, highly robust, low-cost, fast response, label-free detection and hence they are widely studied in various fields such as medical diagnostics, drug detection, food safety control and environment monitoring for the investigation mainly on the bio-molecular interaction and recognition of target analytes [1]–[3].

The optical phenomenon named as SPR is generally defined as the coupling/excitation between the surface plasmon wave and the electromagnetic wave propagating at the interface between a dielectric medium and a conductor [4]. The resonant wavelength of a biosensor is extremely sensitive to the refractive index changes of surrounding analyte at the sensing region. Since Kretschmann and Raether investigated and revealed the SPR phenomenon in 1960s [5], the prism-based SPR biosensors are widely used in practical applications and research developments. Traditional prism-based SPR biosensor has its own cons like bulk size, complicated design and structure, high cost and low reliability [6], [7], even though their sensing performance is good enough to detect small variations of the refractive index of the analyte [8].

In order to overcome these disadvantages, optical fiber SPR biosensor was proposed as it has the design flexibility and also compact in size [4]. Unlike the conventional prism-based SPR biosensor configuration, in optical fiber SPR biosensor, prism is replaced by the fiber and the excitation of surface plasmons is formed through the fiber coupling rather than the prism coupling. Therefore, low cost, highly integrable and portable optical biosensors are achieved. Moreover, real-time monitoring can also be realised by optical fiber based biosensors. For the first time, in 1993, Jorgenson proposed the optical fiber SPR biosensor with a maximum refractive index measurement resolution of 7.5×10^{-4} RIU at the wavelength of 900 nm [4]. Thereafter, a large number of different types of optical fiber based SPR biosensors for various applications have been studied and reported both theoretically and experimentally [9]. In order to achieve high sensitivity and narrow loss spectrum, multi-mode fibers were used instead of single mode fibers [10]. For different fabrication methods and setups, the transmission-based SPR fiber biosensor and the reflection based SPR fiber sensors were both reported by Papiya Dhara *et al.*, in 2015 [11]. Recently, with the development of photonic crystal fiber (PCF), PCF based biosensor has been one of the most popular devices

for biochemical sensing due to its versatile applications and the ability to control the optical characteristics of the fiber through different photonic crystal structural design and structure parameters [12], [13]. In 2007, Hassani and Skorobogatiy reported a refractive index based SPR-PCF biosensor [14]. It provides a new coupling mechanism concept for SPR sensing that can be explained by the propagation constants equivalence of a leaky core-guided mode and a plasmonic mode at the resonant wavelength. Using materials like Polymethyl methacrylate (PMMA) it is possible to fabricate PCFs with optimized structure through different designs, which help to develop PCF based SPR biosensor with various sensing ability, better sensing performance and to detect liquids with wide range of refractive indices [15]. Many different PCF-SPR biosensors with innovative design structures were proposed to enhance the sensing performances. In 2012, multi-core holey fiber was proposed by Shuai *et al.*, for a large range of analyte refractive indices [9]. Later, Wei *et al.*, reported a biosensor using two polarized modes for simultaneous detection in 2013 [16]. Further, in 2016, Yang *et al.*, achieved an extremely high sensitivity of 19009.17 nm/RIU by embedding silver nanowires within a PCF for glucose detection [6]. Moreover, Liu *et al.*, in 2017, proposed a PCF biosensor design with a sensitivity of 7500 nm/RIU achieved through gold-graphene composite film coating [17]. As a different kind of novel microstructured fiber, a solid-core photonic quasi-crystal fiber (PQF) with aperiodic air holes arrangement in the cladding region was proposed and it exhibited unique optical characteristics such as less confinement loss, flat dispersion profile for wide range of wavelength, high dispersion values, etc., [18]. Of late, Aruna Gandhi *et al.*, proposed a biosensor to sense glycerol using a ten-fold PQF with a maximum sensitivity of 6000 nm/RIU [19]. In this direction, we have also recently designed a metal coated (inner side of the holes) six-fold PQF biosensor using PMMA as the cladding material for sensitivity enhancement and structural stabilization [7]. However, one serious downside of PCF-SPR biosensor is the difficulty of coating the metal film in the inner walls of the tiny air holes with the existing PCF fabrication technologies. Hence, the D-shaped PCF biosensor was proposed for the feasibility of fabricating biosensors, as the metal film can be coated on the fiber surface with the side-polishing technology [20]. With all these recent developments in PCF-SPR biosensors, detection of high refractive index liquid analytes is still a challenge in biosensor design.

In this paper, a six-fold PQF biosensor with a trapezoidal channel (TC-PQF) is proposed and theoretically analysed to obtain high sensitivity for the sensing of high refractive index liquid analytes. Its structure is based on the common D-shaped biosensor but has a trapezoidal shaped cross-section channel to infuse the liquid analyte easily. Due to its unique structure, the PQF based sensor has several optical advantages such as flattened zero-dispersion profile for a wide range of wavelength and low confinement loss that will ensure the accuracy and stability during the sensing process [19], [21]. The effect of the different height levels of the liquid analyte on the detection performance of the biosensor has been theoretically investigated through finite element method (FEM).
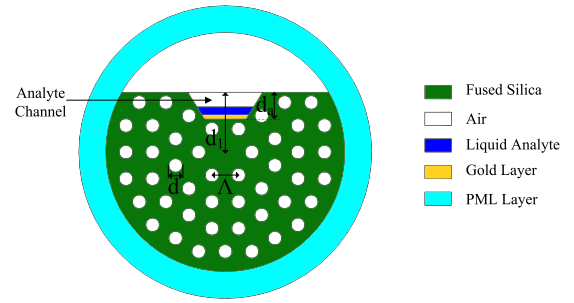

Fig. 1.   Cross-section of the proposed six-fold PQF-SPR biosensor.

II. Geometric Structure and Numerical Modelling

The schematic of the proposed biosensor is shown in Fig. 1. It comprises of 4 layers of air holes arranged in a six-fold PQF structure of air holes diameter of $d = 1~\mu$m with no central air hole. The distance between two holes (pitch), Λ, is 2 μm and the radius of the whole biosensor is set as 9 μm. An open trapezoid shaped analyte channel is situated at the top middle part of the fiber cross-section so that the analyte can be infused in the channel. The height of the trapezoid channel, d_a, is 2 μm. The width of the top wider side and bottom shorter side of the trapezoidal cross-section cavity are $W_{top} = 5.62~\mu$m and $W_{bottom} = 3.12~\mu$m, respectively. An uniform thin gold film layer of thickness $t_{Au} = 50$ nm is coated in the base of the channel for the surface plasmon excitation. The distance between the top of the trapezoid-shaped cross-section and fiber core is $d_1 = 4.5~\mu$m.

Fused silica is considered as the cladding material and the wavelength dependence of the refractive index of the silica glass is calculated by the following Sellmeier equation [22]:

$$n(\lambda) = \sqrt{1 + \frac{B_1{}^2}{\lambda^2 - C_1} + \frac{B_2{}^2}{\lambda^2 - C_2} + \frac{B_3{}^2}{\lambda^2 - C_3}}, \quad (1)$$

where $B_1 = 0.691663$, $B_2 = 0.407943$, $B_3 = 0.897479$, $C_1 = 0.004679~\mu$m^2, $C_2 = 0.013512~\mu$m^2, and $C_3 = 97.934003~\mu$m^2. Here, the λ represents the incident light wavelength in vacuum. Meanwhile, the dielectric constant of the thin gold film is calculated using the Drude model that is characterized as [14]:

$$\varepsilon(\omega) = \varepsilon^\infty - \frac{\omega_p^2}{\omega(\omega + i\omega_c)}, \quad (2)$$

here $\varepsilon^\infty = 9.75$ is the high frequency dielectric function of gold; while $\omega_p = 1.36 \times 10^{16}$ rad/s and $\omega_c = 1.45 \times 10^{14}$ rad/s are the plasma frequency of the metal and scattering frequency of the electrons, respectively. The refractive index of air is set to a value of 1.

There are different types of biochemicals, biomolecules and bio-substances that can be detected using the PQF biosensor as long as the surface plasmon mode is created for the range of refractive indices of the samples that are of interest. In some cases helping agents are required to keep the bio-substance under investigation in the sensing area of the biosensor. For instance, Poly-L-lysine (PLL) is commonly used to immobilise
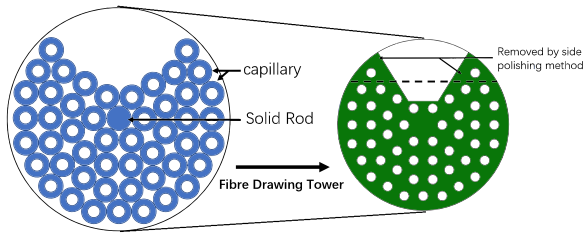
Fig. 2. Stacked preform of the proposed PQF and side polishing method for the top edges removal.
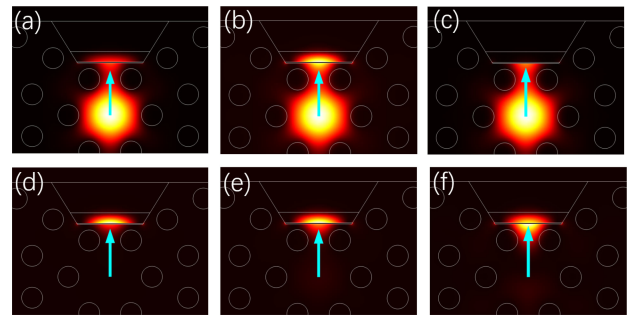

Fig. 3. Light energy flow distributions in the cross-section of PQF-SPR biosensor for different wavelengths for the analyte RI of $n_a = 1.49$ and height 500 nm. (a) and (d) are the FM and PM at 1370 nm (shorter wavelength with respect to the resonance). (b) and (e) are the FM and PM at resonant wavelength of 1492 nm. (c) and (f) are the FM and PM at 1650 nm (longer wavelength with respect to the resonance).

biomolecules such as deoxynucleic acid (DNA) and it will im-mobilise itself to a solid surface. Hence, the molecular inter-actions of DNA can be detected by a PLL bound surface. In general, the PLL and DNA layers have a refractive index range of 1.45 to 1.48 [23]. In our simulations, the refractive index (RI) ranges of the analyte are set within the range of 1.40–1.58 to detect wide range of bio-substances including the sensing of DNA assisted by the PLL.

The proposed structure can be fabricated using the state-of-the-art technique of stack-and-draw [24] and side polishing methods [25]. The fabrication process of proposed biosensor can be based on side-channel PCF fabrication which has been successfully fabricated by Nan Zhang *et al.*, using two steps stack-and-draw process and the channel can be created by re-moving one-sixth of the holy lattice cladding as illustrated in Fig. 2 [26]. During the fiber drawing process, as reported by Nan Zhang *et al.*, [27] the pressure, vacuum and the stability of drawing tower need to be well controlled to keep the struc-ture of the PQF. In order to achieve a trapezoid shape, the side polishing method can be used to remove the two top edges. The rugged surface of the trapezoid base can be processed by a focused high-power laser beam through the cavity to achieve flat bottom surface of the channel. Finally, a thin gold layer can be coated on the sensing surface with a chemical deposition method, described by Jonathan Boehm [28].

To numerically investigate the sensing performance of this biosensor, FEM is used to find the effective refractive indices through COMSOL Multiphysics software. A perfectly matched layer (PML) is considered as the boundary condition for the out-side edges to absorb the radiated light energy for the simulation to mimic the real situation [29].

III. SENSING PERFORMANCE

In any SPR based sensor, it is well known that at the resonant wavelength, the surface plasmon mode (PM) is created through the light energy transfer from the main core-guided fundamental mode (FM) [30].

Simulations results performed on the designed PQF-SPR biosensor for the formation of the PM are shown in Fig. 3. The liquid analyte height was set as 500 nm (25% of the channel height) and the refractive index of the liquid analyte is consid-ered as $n_a = 1.49$. Fig. 3 illustrate both the distribution of the time averaged energy flow of the FM [Fig. 3(a)–(c)] and the PM [Fig. 3(d)–(f)] of the proposed biosensor at 1370 nm [shorter wavelength with respect to the resonance; Fig. 3(a) and (d)],
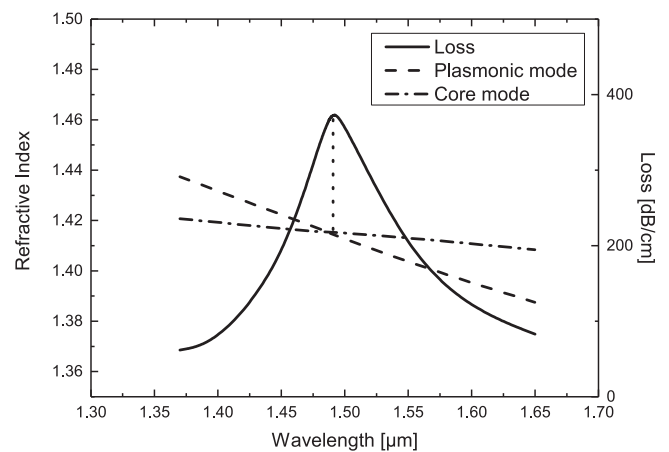

Fig. 4. The confinement loss, dispersion relations of FM and PM of the PQF-SPR biosensor for analyte height of 500 nm (25% of the channel height) and RI $n_a = 1.49$.

1492 nm [resonant wavelength; Fig. 3(b) and (e)] and 1650 nm [longer wavelength with respect to the resonance; Fig. 3(c) and (f)], respectively. The arrows indicate the direction of the elec-tric field. Fig. 3(d)–(f) show the formation of the PM for all three wavelengths, viz., shorter, equal and longer with respect to the resonant wavelength. From Fig. 3(a)–(c), it is clear that part of the FM light energy leaked into the gold film sensing area as PM light signal.

Fig. 4 shows the confinement loss spectrum (solid curve), dispersion relations of the PM (dashed curve) and FM (dot-dashed curve) calculated from the simulations results for the PQF-SPR biosensor. In these calculations, confinement loss can be calculated in dB/cm as [31]:

$$\alpha_{\text{loss}} = 8.686 \times \frac{2\pi}{\lambda} \Im(n_{\text{eff}}) \times 10^4, \qquad (3)$$

where $\Im(n_{\text{eff}})$ is the imaginary part of the effective refractive index of the FM. For the proper sensing and detection pro-cess of the SPR based biosensors, it is important to achieve phase matching condition between the FM and PM [32]. For the proposed PQF-SPR biosensor, the phase matching condition be-tween the FM and PM is found at the resonant wavelength of

1492 nm. The strongest coupling/excitation occurred at this resonant wavelength as the peak of the confinement loss is located at this wavelength as shown in Fig. 4. This clearly indicates that maximum energy transfer of the light signal from FM to PM happened at this resonant wavelength.

For the better performance of a refractive index based SPR biosensor, the energy transferred to the PM should be extremely sensitive to the RI changes of the aqueous analyte [33], [34]. When there are small RI changes in the analyte, the peak of the effective refractive index of the PM should shift its position with respect to the light signal wavelength. As a consequence, the resonant wavelength occurring at the phase matching condition will also shift accordingly.

Fig. 5(a) shows a trend for the family of the confinement loss curves of the analyte's RI in the range of 1.41 to 1.52 when analyte height (H_a) is 500 nm. As the RI of the analyte increases, up to a particular value (1.46) the peak value of the loss curve increases and then goes down. On the other hand, the location of the peak always shifts towards the longer wavelength side. While the peak values go down the loss curves become more and more blunt and getting broader as well.

According to the wavelength interrogation method, the sensitivity of the biosensor can be calculated in nm/RIU using the expression [35]:

$$S_\lambda(\lambda) = \frac{\Delta\lambda_{\text{peak}}}{\Delta n_a}, \qquad (4)$$

where $\Delta\lambda_{\text{peak}}$ is the resonant wavelength shift and Δn_a is the analyte refractive index difference. For example, in Fig. 5(a), the wavelength shift between the confinement loss peaks for RI 1.48 and 1.49 is 48 nm. Hence, the sensitivity of the PQF-SPR biosensor for the analyte RI change from 1.48 to 1.49 is calculated as 4800 nm/RIU. Table I reports the resonant wavelengths and the corresponding sensitivities of the PQF-SPR sensor for various RI values of the analyte.

The maximum calculated resolution of the designed PQF-SPR biosensor is as high as 1.64×10^{-5} RIU for a 0.1 nm peak-wavelength resolution of the instrument within the RI sensing range of 1.41 to 1.52. However, the peak of the confinement loss decreases with the increasing values of the analyte RI and also the peak is not sharp enough to detect the loss peak point for the analyte with refractive index over 1.52. 50% confinement loss bandwidth (calculated as full width at half-maximum (FWHM)) reported in Table I gives the idea how sharp or blunt the confinement loss curves are.

Above simulations results for the PQF-SPR biosensor are reported for a height of 500 nm that is 25% of the channel height. We investigated the performance of the designed PQF-SPR biosensor for different analyte heights in the channel. By decreasing the analyte height to 400 nm (20% of the channel height), we found the possibility to extend the RI sensing range of the PQF-SPR biosensor from $1.41-1.52$ to $1.44-1.58$. Fig. 5(b) shows the confinement loss spectra for the analyte RI varying from 1.44 to 1.58 when H_a is 400 nm and the calculated sensitivity and FWHM loss bandwidth are summarised in Table II. The wavelength shift of the spectrum of the confinement loss peak for the analyte RI of 1.46, 1.47 and 1.48 are
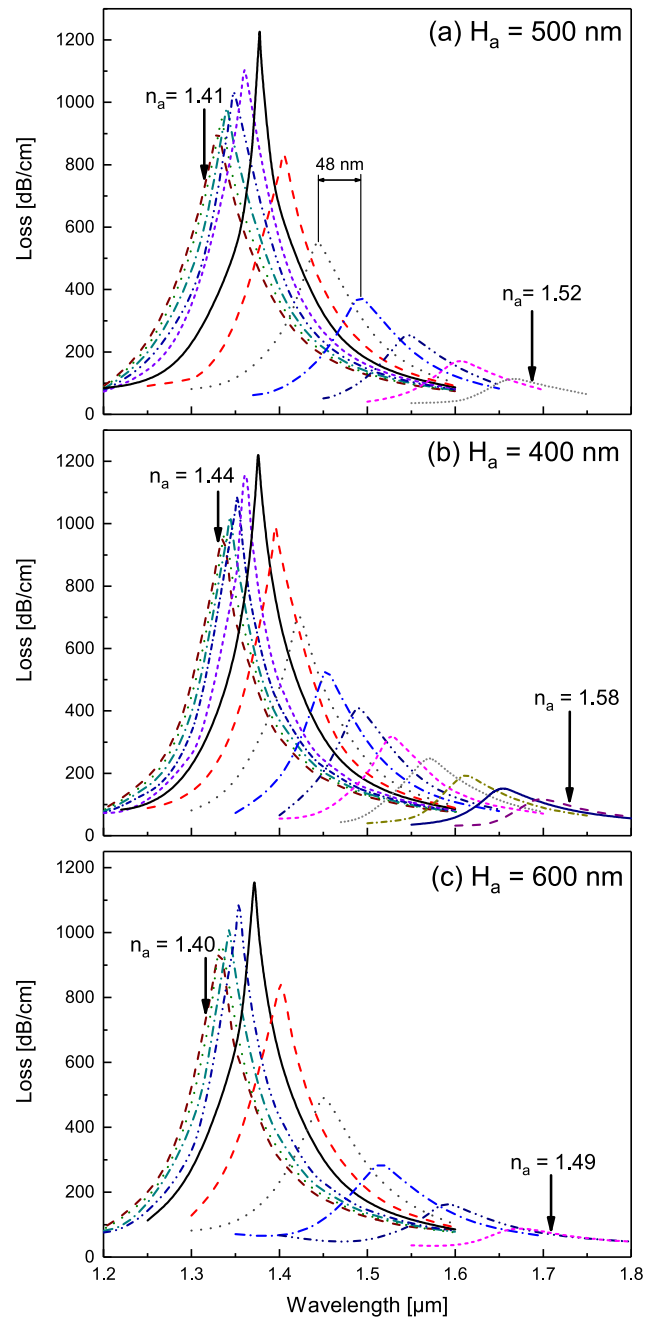

Fig. 5. The loss spectra for the analyte refractive index (n_a) varying from (a) 1.41 to 1.52 in steps of 0.01, (b) 1.44 to 1.58 in steps of 0.01 and (c) 1.40 to 1.49 in steps of 0.01.

too small for precise detection and their sensitivities are lower than 1500 nm/RIU. Hence the designed PQF-SPR biosensor is considered to work with a better sensing performance within the analyte RI range of 1.49 to 1.58 when the analyte height is 400 nm. Thus, the sensing of analyte's RI range extension towards very high values above 1.58 is at the cost of reduced sensitivity. Also another notable information from Table II is that the maximum sensitivity is 27.8% lower than the simulation results of 25% of liquid analyte height (500 nm) and at the same time with an improvement of 28.6% in the detectable analyte's RI range.

TABLE I
SENSITIVITY DATA OF THE PQF-SPR BIOSENSOR (ANALYTE HEIGHT OF
500 NM [25% OF CHANNEL HEIGHT])

Analyte Refractive Index	Resonant Wavelength (nm)	Peak Loss (dB/cm)	FWHM Loss Bandwidth (nm)	Sensitivity (nm/RIU)
1.41	1330	922.8	89	400
1.42	1334	948.3	87	600
1.43	1340	989.7	84	800
1.44	1348	1042.8	78	1200
1.45	1360	1126.6	76	1760
1.46	1378	1229.4	47	2740
1.47	1405	831.7	83	3900
1.48	1444	547.9	98	4800
1.49	1492	372.5	110	5500
1.50	1548	252.6	119	5900
1.51	1606	170.4	134	6100
1.52	1667	113.7	161	–

TABLE II
SENSITIVITY PROFILE OF PROPOSED BIOSENSOR (ANALYTE HEIGHT OF 400 NM
[20% OF CHANNEL HEIGHT])

Analyte Refractive Index	Resonant Wavelength (nm)	Peak Loss (dB/cm)	FWHM Loss Bandwidth (nm)	Sensitivity (nm/RIU)
1.44	1334	942.6	88	300
1.45	1337	962.8	88	700
1.46	1344	1022.6	76	800
1.47	1352	1084.1	75	1000
1.48	1362	1155.8	65	1400
1.49	1376	1246.9	54	2000
1.50	1396	993.4	75	2700
1.51	1423	702.8	87	3100
1.52	1454	531.7	94	3600
1.53	1490	408.9	102	3900
1.54	1529	318.2	105	4100
1.55	1570	247.8	117	4200
1.56	1612	193.5	119	4200
1.57	1654	151.1	133	4400
1.58	1698	117.6	152	–

TABLE III
SENSITIVITY PROFILE OF PROPOSED BIOSENSOR (ANALYTE HEIGHT OF 600 NM
[30% OF CHANNEL HEIGHT])

Analyte Refractive Index	Resonant Wavelength (nm)	Peak Loss (dB/cm)	FWHM Loss Bandwidth (nm)	Sensitivity (nm/RIU)
1.40	1330	923.8	88	500
1.41	1335	954.4	87	800
1.42	1343	1013.6	81	1100
1.43	1354	1085.2	73	1800
1.44	1372	1158.5	61	2900
1.45	1401	844.8	84	5000
1.46	1451	490.4	109	6400
1.47	1515	286.8	130	7500
1.48	1590	162.5	151	8000
1.49	1670	88.4	226	–

index for all the three different heights of the analyte. Loss resonant wavelengths of the loss spectra for three different analyte heights are plotted in Fig. 6(b). The loss resonant wavelength values increase linearly with the increasing values of the refractive index of the analyte. Straight line fitting for the loss resonant wavelengths for the analyte heights H_a equals 400 nm, 500 nm and 600 resulted with the slopes of 3.6582, 4.9036 and 6.06; y−intercepts of −4.0951, −5.8006 and −7.3781; and R−squared values of 0.99051, 0.9856 and 0.97653, respectively. Fig. 6(b) shows the fitted three straight lines for the loss resonant wavelengths data. R−squared values as close to 1 indicate good straight line fit for the loss resonant wavelengths data for all three heights of the analyte. Slopes calculated from the straight lines fit are the average sensitivity of the biosensor for different analyte heights. Using the sensitivity (S) value and the FWHM bandwidths data, we can calculate the figure of merit (FOM) [36] of the designed biosensor as

$$\text{FOM} = \frac{\text{S } (\mu\text{m/RIU})}{\text{FWHM Bandwidth } (\mu\text{m})}. \qquad (5)$$

It should be noted that, as the FWHM bandwidth getting broadened to the longer wavelength, the FOM of the sensor will be degraded. As it is presented in Fig. 6(c), the average FOM obtained for liquid heights of 400 nm, 500 nm and 600 nm are respectively, 43.7 /RIU, 55.8 /RIU and 62.2 /RIU and these values are higher than the FOM reported in [37], [38].

Simulations performed for lower heights of the liquid analyte for 100 nm, 200 nm and 300 nm (within 15% of the channel height) to investigate the sensing performance of the sensor. As illustrated in Fig. 7, the wavelength shifts of resonant peaks for different RI of the analytes with the same liquid height were found to be very small and this can be very difficult to be measured using spectrometer. According to the results reported in Fig. 7, it is clear that the sensitivities are too low (wavelengths shift are all less than 5.5 nm) for the differences in the analyte RI when the analyte height is lower than 400 nm (within 15% of the channel height). Thus minimum 15% liquid height level with respect to the total analyte cavity height is the threshold requirement for the PQF-SPR biosensor to exhibit accurate detection and better sensing performance.
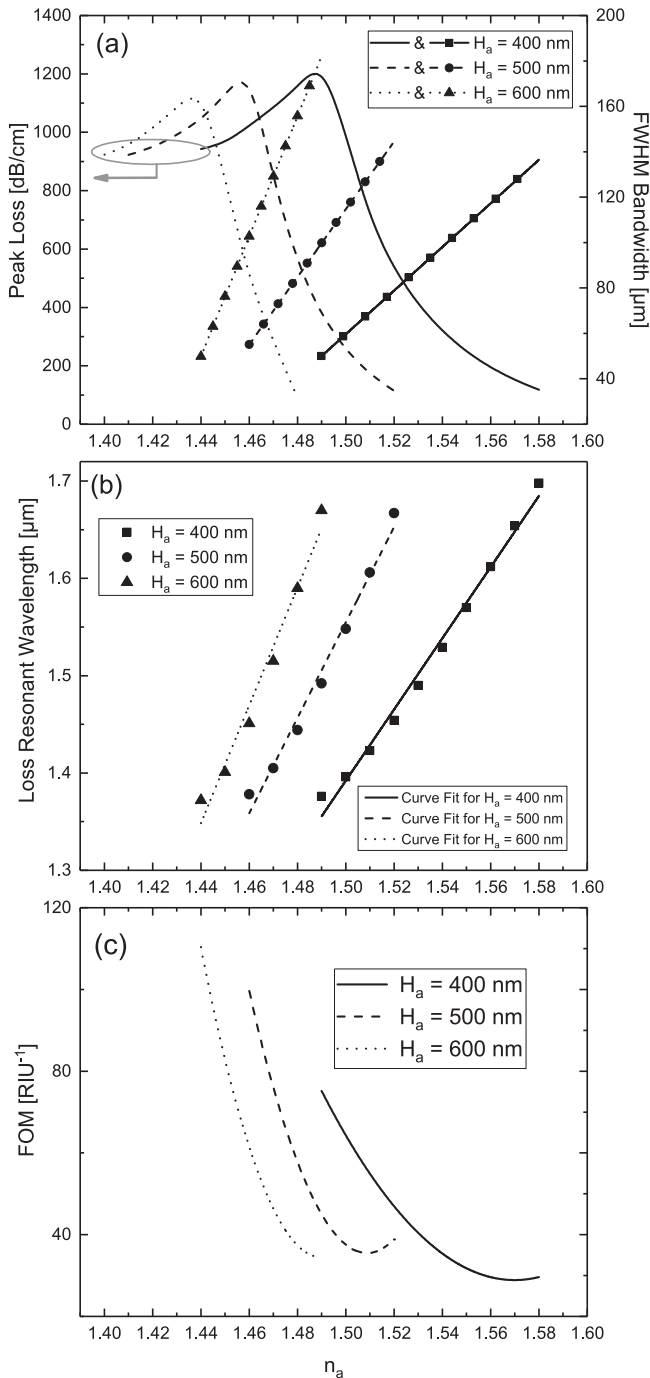
Investigation on the performance of the PQF-SPR biosensor was performed for an analyte height to 600 nm (30% of the channel height). In this case as well, the biosensor exhibited similar relationship between the analyte's RI sensing range and the maximum sensitivity, see Fig. 5(c). The analyte's RI sensing range for 600 nm of H_a is found to be from 1.40 to 1.49 and the maximum sensitivity is calculated as 8000 nm/RIU, see Table III. Moreover, for an analyte height of 1000 nm (50% of the channel height), the highest value of sensitivity is calculated as 17000 nm/RIU. This increased sensitivity of the designed sensor is available at the cost of limited RI sensing range of 1.40 to 1.44.

The peak losses and FWHM bandwidths of the loss spectra corresponding to different RI of the analyte when the liquid height H_a is 400 nm, 500 nm and 600 nm are shown in Fig. 6(a). For all the three different heights of the analyte, we can see the trend of the peak loss increasing up to a certain value of the refractive index and then decreasing for further increase of the refractive index value. While the FWHM bandwidths linearly increasing for increasing values of the analyte refractive
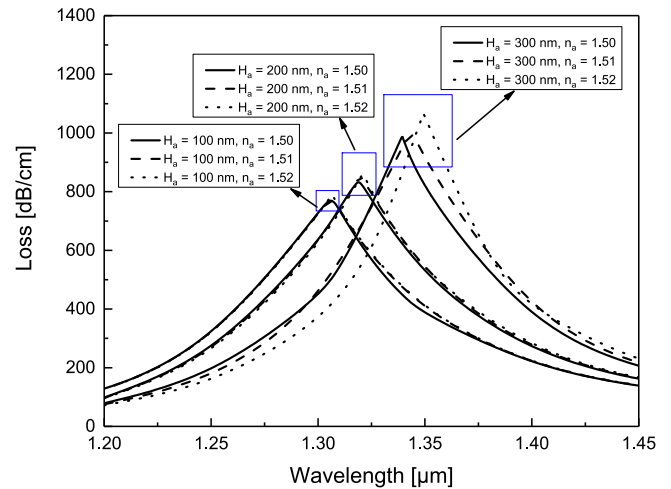
Fig. 7. The loss spectra for the analyte RI varying from 1.50 to 1.52 with different analyte heights of 100 nm, 200 nm and 300 nm.

distances of 1.9 μm, 2.0 μm and 2.1 μm, different gold layer thickness values of 40 nm, 50 nm and 60 nm for the analyte RI values of 1.50 and 1.51, when the liquid height is 400 nm are depicted in Fig. 8. In Fig. 8(a), it can be seen that when the air holes diameter is 0.9 μm, the shift of the resonant wavelength is only 15 nm which resulted in a low sensitivity value of 1500 nm/RIU. On the other hand, when the air holes diameter is set to 1.1 μm, the shift of the resonant wavelength is up to 34 nm. Although it can provide a high sensitivity of 3400 nm/RIU for the analytes' RI of 1.50 and 1.51, the loss spectra are not very sharp. In Fig. 8(b), it can be seen that the resonant wavelength shift is increased with the increase of pitch distance, whereas the loss is decreased. In Fig. 8(c), the resonant wavelength shift for three different gold coating thickness of 40 nm, 50 nm, 60 nm were 25 nm, 27 nm and 22 nm, respectively. Either increase or decrease of gold coating thickness from the original value of 50 nm reduces the sensitivity of the biosensor. Hence, in order to achieve the best sensing performance of the PQF-SPR biosensor, the values of air holes diameter, pitch and gold coating thickness are to be as near as the designed values of 1.0 μm, 2.0 μm and 50 nm, respectively to achieve a resonant wavelength shift of 27 nm and the corresponding sensitivity of 2700 nm/RIU.

V. TOLERANCE STUDY OF DESIGN PARAMETERS

We investigated the tolerance of the TC-PQF biosensor as it is practically difficult to fabricate the biosensor exactly as the physical parameters in the design, such as the air holes diameter $d = 1$ μm, trapezoid channel cavity depth $d_a = 2$ μm, top and bottom widths $W_{top} = 5.62$ μm and $W_{bottom} = 3.12$ μm and the side-polishing depth $d_1 = 4.5$ μm, as shown in Fig. 1. Under the current condition of PCF fabrication technology, $\pm 2\%$ to $\pm 5\%$ variations on the designed parameters should be considered as the fabrication tolerance [39]. First we consider the effect of air holes diameter variations for the sensing performance reported for 400 nm (20% of cavity height) liquid analyte height. Fig. 9(a) shows the effect of air holes diameter variations on
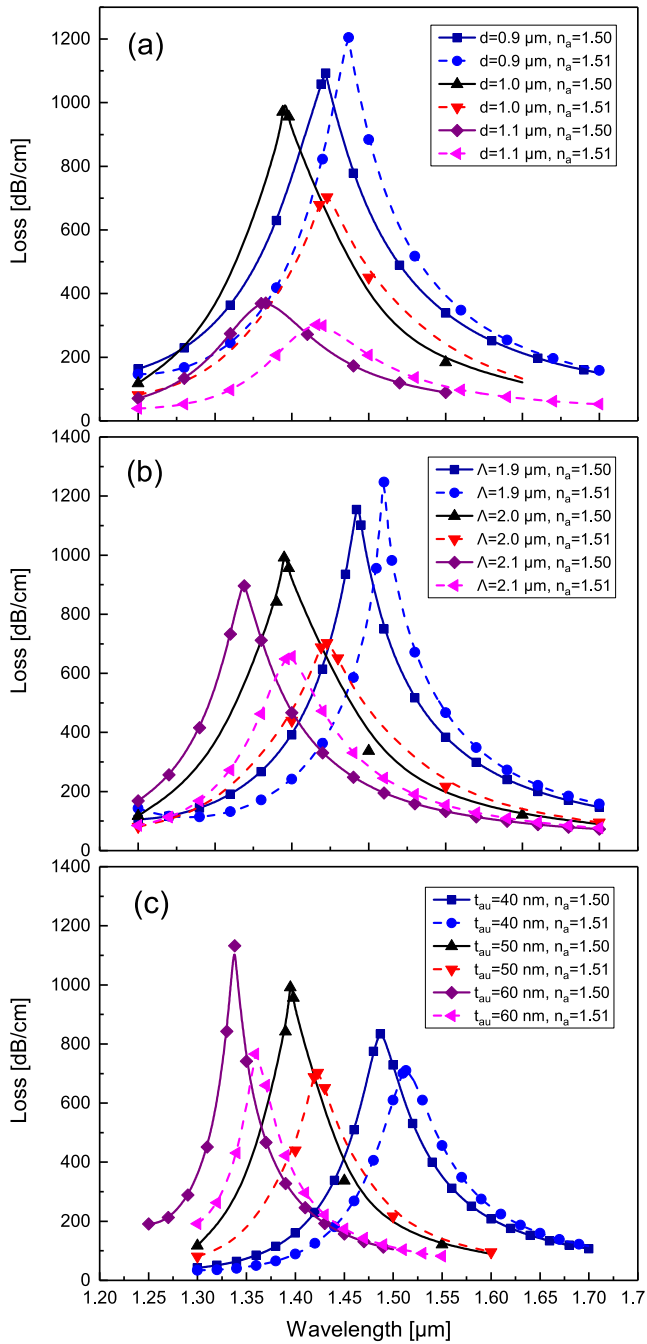

Fig. 6. (a) Peak loss and FWHM Bandwidth for various analyte's RI. (b) Loss resonant wavelengths and straight lines fit. (c) FOM versus analyte's RI for liquid heights $H_a = 400$ nm, 500 nm and 600 nm, respectively.

IV. EFFECT OF VARIATIONS IN AIR HOLES DIAMETER

Changing the structural parametric values of the PQF-SPR biosensor, such as variations in the air holes distance/air holes diameter or using different dielectric/metal materials can influence the sensing performance. Fig. 8 shows the effect of different structure parameters on the sensing performance of the PQF-SPR biosensor. The confinement loss spectra for different air holes diameters values from 0.9 to 1.1 μm, different pitch

Fig. 8. The loss spectra for (a) three different air holes diameters, 0.9 μm, 1.0 μm, 1.1 μm, (b) three different pitch distances between two adjacent air holes, 1.9 μm, 2.0 μm, 2.1 μm, and (c) three different thin gold coating thickness values, 40 nm, 50 nm, 60 nm with a liquid analyte height of 400 nm and RI of 1.50 and 1.51.

the loss spectra of the designed biosensor which indicates that there is −10 nm (+5% change in the air holes diameter; dashed curve) and +12 nm (−5% change in the air holes diameter; dotted curve) relative resonant wavelength shift of the confinement loss peak with respect to the designed parameter value of 1 μm shown as solid curve.

Fig. 9(b) shows the simulations results when the cavity depth is not exactly same as the designed sensor. If the cavity depth
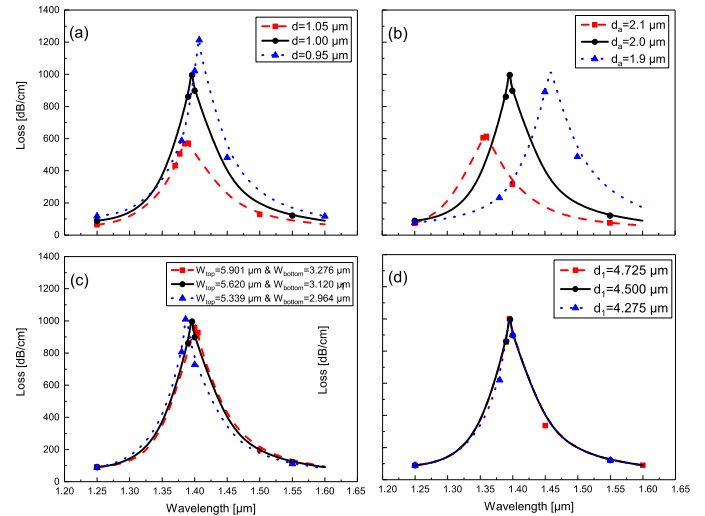

Fig. 9. The investigation on fabrication tolerance of (a) air holes diameter, (b) analyte channel depth, (c) top and bottom base length of trapezoid channel, and (d) side polishing depth.

is having variations of +5% and −5% with respect to the designed RI value of 1.5 shown as solid curve in Fig. 9(b), then the confinement loss peak resonant wavelength shifts are 36 nm (dashed) and 64 nm (dotted), respectively. Furthermore, the effects due to the variations in the trapezoidal cavity bottom and top widths are having variations from the original designed values (solid curve), then the resultant loss spectra are shown in Fig. 9(c) for +5% variation as dashed curve and for −5% variation as dotted curve. Finally for the practical fabrication variations of the distance between the cavity and the centre of the PQF, Fig. 9(d), shows for +5% variation as dashed curve and for −5% variation as dotted curve, with respect to the solid curve for the designed value. It can be seen that the variations occurring in side-polishing depth have negligible wavelength shift from the designed parameter. In conclusion from this tolerance study, one can see that almost all physical parameters variations due to practical limitations in fabricating the designed TC-PQF sensor are resulting a sensing performance very close to the simulations results of the designed TC-PQF sensor.

VI. CONCLUSION

In this paper, we have proposed a six-fold photonic quasi-crystal fiber with a trapezoidal analyte channel to detect the higher refractive index liquids. The numerical results show that the PQF-SPR biosensor could achieve a maximum sensitivity of 4400 nm/RIU (RI = 1.44 to 1.58), 6100 nm/RIU (RI = 1.41 to 1.52), 8000 nm/RIU (RI = 1.40 to 1.49) and 17000 nm/RIU (RI = 1.40 to 1.44) with a liquid analyte height of 20%, 25%, 30% and 50% of the channel height, respectively. We found that the sensitivity of the TC-PQF biosensor is increased as the liquid height raising, however, the sensing range will reduce. Hence, we can corroborate that the analyte liquid height has great influence on both the biosensor's sensitivity and the ability of sensing RI range. Using the designed TC-PQF biosensor, an increment of 28.6% in the analyte RI sensing range can be

achieved by relatively decreasing the analyte height by 100 nm value and of course at a cost of 27.8% decrement in the sensitivity, with respect to the analyte liquid height variations between 20% and 25% height. If the liquid analyte height is below 20% of the channel cavity height, then their is no significant difference in the resonant wavelength shift of the confinement loss peaks, which can be the threshold limit of the applications of the designed PQF-SPR sensor. We believe that this PQF-SPR biosensor could be a potential sensing device for high refractive index bio-chemicals.

REFERENCES

[1] M. R. Hasan *et al.*, "Spiral photonic crystal fiber-based dual-polarized surface plasmon resonance biosensor," *IEEE Sens. J.*, vol. 18, no. 1, pp. 133–140, Jan. 2018.
[2] D. J. J. Hu and H. P. Ho, "Recent advances in plasmonic photonic crystal fibers: Design, fabrication and applications," *Adv. Opt. Photon.*, vol. 9, pp. 257–314, 2017.
[3] B. D. Gupta and R. Kant, "Recent advances in surface plasmon resonance based fiber optic chemical and biosensors utilizing bulk and nanostructures," *Opt. Laser Technol.*, vol. 101, pp. 144–161, 2018.
[4] Y. Zhao, Z.-q. Deng, and J. Li, "Photonic crystal fiber based surface plasmon resonance chemical sensors," *Sens. Actuators B, Chem.*, vol. 202, pp. 557–567, 2014.
[5] E. Kretschmann and H. Raether, "Notizen: Radiative decay of non radiative surface plasmons excited by light," *Zeitschrift für Naturforschung A*, vol. 23, pp. 2135–2136, 1968.
[6] X. Yang, Y. Lu, M. Wang, and J. Yao, "A photonic crystal fiber glucose sensor filled with silver nanowires," *Opt. Commun.*, vol. 359, pp. 279–284, 2016.
[7] G. Melwin *et al.*, "Designing a biosensor using a stampli photonic quasi-crystal fiber," in *Proc. 6th IASTED Int. Conf. Model. Simul.*, 2016, pp. 215–217.
[8] Y.-J. He, "Novel and high-performance LSPR biochemical fiber sensor," *Sens. Actuators B, Chem.*, vol. 206, pp. 212–219, 2015.
[9] B. Shuai, L. Xia, Y. Zhang, and D. Liu, "A multi-core holey fiber based plasmonic sensor with large detection range and high linearity," *Opt. Express*, vol. 20, pp. 5974–5986, 2012.
[10] N. Luan and J. Yao, "Surface plasmon resonance sensor based on exposed-core microstructured optical fiber placed with a silver wire," *IEEE Photon. J.*, vol. 8, no. 1, Feb. 2016, Art. no. 4800508.
[11] P. Dhara, M. Olivero, A. Vallan, G. Perrone, and V. K. Singh, "Transmission and reflection spr disposable fibre probes for bio-chemical sensing," in *Proc. Int. Conf. BioPhotonics*, 2015, pp. 1–5.
[12] A. E. Khalil *et al.*, "Highly sensitive photonic crystal fiber biosensor based on titanium nitride," *Opt. Quantum Electron.*, vol. 50, p. 158, 2018.
[13] S. Chu *et al.*, "Designing a biosensor using a photonic quasi-crystal fiber with fan-shaped analyte channel," in *Proc. Asian Simul. Conf.*, 2017, pp. 529–537.
[14] A. Hassani and M. Skorobogatiy, "Design criteria for microstructured-optical-fiber-based surface-plasmon-resonance sensors," *J. Opt. Soc. Amer. B*, vol. 24, pp. 1423–1429, 2007.
[15] A. A. Rifat *et al.*, "Photonic crystal fiber-based surface plasmon resonance sensor with selective analyte channels and graphene-silver deposited core," *Sensors*, vol. 15, pp. 11 499–11 510, 2015.
[16] Q. Wei, L. Shu-Guang, X. Jian-Rong, X. Xü-Jun, and Z. Lei, "Numerical analysis of a photonic crystal fiber based on two polarized modes for biosensing applications," *Chin. Phys. B*, vol. 22, 2013, Art. no. 074213.
[17] C. Liu *et al.*, "Numerical analysis of a photonic crystal fiber based on a surface plasmon resonance sensor with an annular analyte channel," *Opt. Commun.*, vol. 382, pp. 162–166, 2017.
[18] S. Sivabalan and J. P. Raina, "High normal dispersion and large mode area photonic quasi-crystal fiber stretcher," *IEEE Photon. Technol. Lett.*, vol. 23, no. 16, pp. 1139–1141, Aug. 2011.
[19] M. S. A. Gandhi, S. Sivabalan, P. R. Babu, and K. Senthilnathan, "Designing a biosensor using a photonic quasi-crystal fiber," *IEEE Sens. J.*, vol. 16, no. 8, pp. 2425–2430, Apr. 2016.
[20] Y. Ying *et al.*, "Recent research progress of optical fiber sensors based on d-shaped structure," *Opt. Laser Technol.*, vol. 90, pp. 149–157, 2017.
[21] S. Kim, C.-S. Kee, and J. Lee, "Novel optical properties of six-fold symmetric photonic quasicrystal fibers," *Opt. Express*, vol. 15, pp. 13221–13226, 2007.
[22] E. K. Akowuah *et al.*, "Numerical analysis of a photonic crystal fiber for biosensing applications," *IEEE J. Quantum Electron.*, vol. 48, no. 11, pp. 1403–1410, Nov. 2012.
[23] L. Rindorf *et al.*, "Photonic crystal fiber long-period gratings for biochemical sensing," *Opt. Express*, vol. 14, pp. 8224–8231, 2006.
[24] P. Russell, "Photonic crystal fibers," *Science*, vol. 299, pp. 358–362, 2003.
[25] N. Ashok and W. Shin, "Effective d-shape fiber with air hole assistant design for birefringence analysis," *Optik*, vol. 162, pp. 27–34, 2018.
[26] N. Zhang *et al.*, "Ultra-sensitive chemical and biological analysis via specialty fibers with built-in microstructured optofluidic channels," *Lab Chip*, vol. 18, pp. 655–661, 2018.
[27] N. Zhang *et al.*, "Side-channel photonic crystal fiber for surface enhanced raman scattering sensing," *Sens. Actuators B, Chem.*, vol. 223, pp. 195–201, 2016.
[28] J. Boehm, A. François, H. Ebendorff-Heidepriem, and T. M. Monro, "Chemical deposition of silver for the fabrication of surface plasmon microstructured optical fibre sensors," *Plasmonics*, vol. 6, pp. 133–136, 2011.
[29] X. Yang, Y. Lu, L. Duan, B. Liu, and J. Yao, "Temperature sensor based on hollow fiber filled with graphene-Ag composite nanowire and liquid," *Plasmonics*, vol. 12, pp. 1805–1811, 2017.
[30] P. Leonard, S. Hearty, J. Quinn, and R. OKennedy, "A generic approach for the detection of whole listeria monocytogenes cells in contaminated samples using surface plasmon resonance," *Biosens. Bioelectron.*, vol. 19, pp. 1331–1335, 2004.
[31] X. Chen, L. Xia, and C. Li, "Surface plasmon resonance sensor based on a novel d-shaped photonic crystal fiber for low refractive index detection," *IEEE Photon. J.*, vol. 10, no. 1, Feb. 2018, Art. no. 6800709.
[32] J. N. Dash and R. Jha, "SPR biosensor based on polymer PCF coated with conducting metal oxide," *IEEE Photon. Technol. Lett.*, vol. 26, no. 6, pp. 595–598, Mar. 2014.
[33] H. Lu, X. Liu, and D. Mao, "Plasmonic analog of electromagnetically induced transparency in multi-nanoresonator-coupled waveguide systems," *Phys. Rev. A*, vol. 85, 2012, Art. no. 053803.
[34] Y. Liu *et al.*, "Theoretical design of plasmonic refractive index sensor based on the fixed band detection," *IEEE J. Sel. Topics Quantum Electron.*, vol. 25, no. 2, Mar./Apr. 2019, Art. no. 4600206.
[35] A. A. Rifat, R. Ahmed, G. A. Mahdiraji, and F. R. M. Adikan, "Highly sensitive d-shaped photonic crystal fiber-based plasmonic biosensor in visible to near-ir," *IEEE Sens. J.*, vol. 17, no. 9, pp. 2776–2783, May 2017.
[36] Q. Liu, S. Li, H. Chen, Z. Fan, and J. Li, "Photonic crystal fiber temperature sensor based on coupling between liquid-core mode and defect mode," *IEEE Photon. J.*, vol. 7, no. 2, Apr. 2015, Art. no. 4500509.
[37] P. Chen, Y.-J. He, X.-S. Zhu, and Y.-W. Shi, "Surface plasmon resonance sensor based on ethylene tetra-fluoro-ethylene hollow fiber," *Sensors*, vol. 15, pp. 27917–27929, 2015.
[38] B.-H. Liu, Y.-X. Jiang, X.-S. Zhu, X.-L. Tang, and Y.-W. Shi, "Hollow fiber surface plasmon resonance sensor for the detection of liquid with high refractive index," *Opt. Express*, vol. 21, pp. 32349–32357, 2013.
[39] M. R. Hasan, M. I. Hasan, and M. S. Anower, "Tellurite glass defect-core spiral photonic crystal fiber with low loss and large negative flattened dispersion over s + c + l + u wavelength bands," *Appl. Opt.*, vol. 54, pp. 9456–9461, 2015.

Suoda Chu received the B.Eng. degree in communication engineering from the Jinling College, Nanjing University, Nanjing, China, in 2010, and the M.Sc. degree in microwave and wireless communication engineering from Cardiff University, Cardiff, U.K., in 2014. He is currently working toward the Ph.D. degree with the School of Engineering, University of Aberdeen, Aberdeen, U.K.

K. Nakkeeran (SM'18) received the B.Eng. degree from the Coimbatore Institute of Technology, Coimbatore, India, in 1993, and the M.Tech. and Ph.D. degrees from Anna University, Chennai, India, in 1995 and 1998, respectively. In 1999, he joined the Institute of Mathematical Sciences, Chennai, where he was a Postdoctoral Fellow for ten months. In 1999, he became a Research Associate with the Department of Physics, University of Burgundy, Dijon, France. In 2002, he became a Postdoctoral Fellow with the Department of Electronic and Information Engineering, The Hong Kong Polytechnic University. In 2005, he joined the School of Engineering, University of Aberdeen, Aberdeen, U.K., where he has been a Senior Lecturer since 2011. His research interests include solitons, fiber lasers, fiber sensors, modeling and simulations of optical devices, long-haul optical fiber communications, and nonlinear science. He is a senior member of the Optical Society of America and a member of the Institution of Engineering and Technology.

Sumeet S. Aphale (SM'18) received the B.E. degree from the University of Pune, Pune, India, in 1999, and the M.S. and Ph.D. degrees from the University of Wyoming, Laramie, WY, USA, in 2003 and 2005, respectively, all in electrical engineering with a focus on robotics and control. He is currently a Senior Lecturer with the School of Engineering, University of Aberdeen, Aberdeen, U.K. He has held postdoctoral research positions with the ARC Centre of Excellence for Complex Dynamic Systems and Control, University of Newcastle (from 2006 to 2008) and with the Centre for Applied Dynamics Research, University of Aberdeen (from 2008 to 2009). He has authored more than 60 papers in peer-reviewed journals and conferences. His research interests include nanopositioning, drill-string dynamics, vibration control, flexible manipulators, Gough–Stewart platforms, biomedical devices, and fiber-optic sensors. He is an Associate Editor for the IEEE Control Systems Society's Conference Editorial Board. He is an Associate Editor for *Shock and Vibration* and *Frontiers of Mechanical Engineering* (Mechatronics Section). He is a member of the Institution of Engineering and Technology. He is a Chartered Engineer.

Abdosllam M. Abobaker (M'07) received the High Diploma in electronic engineering from the Higher Institute of Electricity, Zliten, Libya, in September 1995, the M.Eng. degree in engineering (communication and computer) from the National University of Malaysia, Bangi Selangor, Malaysia, in November 2003, and the Ph.D. degree in engineering from the University of Aberdeen, Aberdeen, U.K., in November 2009. In 2010, he joined the College of Electronic Technology, Bani Walid, Libya, as a faculty member and became a Dean of the college in 2011. He became the President of the Constituent Committee for the establishment of the Supreme Council of Technical and Vocational Education, Ministry of Higher Education, Libya, in May 2012. His research interests include solitons, fiber lasers, long-haul optical fiber communications, and nonlinear science modeling and simulations of optical devices. He is a member of the Optical Society of America.

P. Ramesh Babu received the M.Sc., M.Phil., and Ph.D. degrees in physics from the University of Madras, Chennai, India. He is currently a Professor with the Vellore Institute of Technology, Vellore, India. His research interests include fiber Bragg gratings, optical fiber communications, photonic crystal fibers, pulse compression, metamaterials, and Bose–Einstein condensation.

K. Senthilnathan received the M.Sc. and M.Phil. degrees in physics from the University of Madras, Chennai, India, and the Ph.D. degree from Anna University, Chennai. He is currently a Professor with the Vellore Institute of Technology, Vellore, India. His research interests include optical fibers, fiber Bragg gratings, photonic crystal fibers, pulse compression, Bose–Einstein condensation, and metamaterials.